Toward a Seasonally Ice-Covered Arctic Ocean: Scenarios from the IPCC AR4 Model Simulations

XIANGDONG ZHANG AND JOHN E. WALSH

International Arctic Research Center, University of Alaska Fairbanks, Fairbanks, Alaska

(Manuscript received 16 May 2005, in final form 23 September 2005)

ABSTRACT

The sea ice simulations by the Intergovernmental Panel on Climate Change Fourth Assessment Report (IPCC AR4) models for the climate of the twentieth century and for global warming scenarios have been synthesized. A large number of model simulations realistically captured the climatological annual mean, seasonal cycle, and temporal trends of sea ice area over the Northern Hemisphere during 1979–99, although there is considerable scatter among the models. In particular, multimodel ensemble means show promising estimates very close to observations for the late twentieth century. Model projections for the twenty-first century demonstrate the largest sea ice area decreases generally in the Special Report on Emission Scenarios (SRES) A1B and A2 scenarios compared with the B1 scenario, indicating large multimodel ensemble mean reductions of $-3.54 \pm 1.66 \times 10^5$ km^2 decade^{-1} in A1B, $-4.08 \pm 1.33 \times 10^5$ km^2 decade^{-1} in A2, and $-2.22 \pm 1.11 \times 10^5$ km^2 decade^{-1} in B1. The corresponding percentage reductions are 31.1%, 33.4%, and 21.6% in the last 20 yr of the twenty-first century, relative to 1979–99. Furthermore, multiyear ice coverage decreases rapidly at rates of $-3.86 \pm 2.07 \times 10^5$ km^2 decade^{-1} in A1B, $-4.94 \pm 1.91 \times 10^5$ km^2 decade^{-1} in A2, and $-2.67 \pm 1.7107 \times 10^5$ km^2 decade^{-1} in B1, making major contributions to the total ice reductions. In contrast, seasonal (first year) ice area increases by $1.10 \pm 2.46 \times 10^5$ km^2 decade^{-1}, $1.99 \pm 1.47 \times 10^5$ km^2 decade^{-1}, and $1.05 \pm 1.9247 \times 10^5$ km^2 decade^{-1} in the same scenarios, leading to decreases of 59.7%, 65.0%, and 45.8% of the multiyear ice area, and increases of 14.1%, 27.8%, and 11.2% of the seasonal ice area in the last 20 yr of this century. Statistical analysis shows that many of the models are consistent in the sea ice change projections among all scenarios. The results include an evaluation of the 99% confidence interval of the model-derived change of sea ice coverage, giving a quantification of uncertainties in estimating sea ice changes based on the participating models. Hence, the seasonal cycle of sea ice area is amplified and an increased large portion of seasonally ice-covered Arctic Ocean is expected at the end of the twenty-first century. The very different changes of multiyear and seasonal ice may have significant implications for the polar energy and hydrological budgets and pathways.

1. Introduction

As an active and responsive component of the climate system, sea ice serves as an integrative indicator of global warming. Sea ice is a key contributor to the albedo feedback in the surface air temperature increase and global warming amplification (e.g., Manabe and Stouffer 1980). In turn, the overall sea ice reduction is a consequence of the surface temperature rise. In association with increases of surface air temperature in the polar regions, sea ice area and volume reductions have been well documented by observational and modeling studies (e.g., Chapman and Walsh 1993; Rind et al. 1995; Parkinson et al. 1999; Rothrock et al. 1999; Wadhams and Davis 2000; Comiso 2002; Cavalieri and Parkinson 2003; Serreze et al. 2003; Johannessen et al. 2004).

Global warming will very likely continue under various possible emissions scenarios even though many countries have agreed to limit or reduce emissions of greenhouse gases under the Kyoto Protocol. The likelihood of continued warming makes the shrinkage of Arctic sea ice a significant climate issue, raising the question of how much of the Arctic Ocean will be covered by sea ice in the twenty-first century and beyond. An assessment, albeit very limited, of Arctic sea ice changes was made in the Third Assessment Report (TAR) of the Intergovernmental Panel on Climate Change (IPCC; Houghton et al. 2001) and in the Arctic

Corresponding author address: Xiangdong Zhang, International Arctic Research Center, University of Alaska Fairbanks, Fairbanks, AK 99775.
E-mail: xdz@iarc.uaf.edu

Climate Impact Assessment (ACIA 2004), in which a large range of uncertainty was noted in the climate models that produce the climate change projections of sea ice. Moreover, since 1996, the IPCC developed a new set of emissions scenarios described in the IPCC Special Report on Emission Scenarios (SRES; Nakicenovic and Swart 2000), representing alternative future emissions outcomes based on a range of assumptions regarding population, economic growth, energy-related technology, etc. However, most modeling centers adopted these scenarios too late for them to be incorporated into the climate model simulations for TAR. Only a small number of modeling centers conducted simulations under a few of various marker scenarios for the TAR (Houghton et al. 2001, their Table 9.1).

The most comprehensive set of multimodel and multiscenario simulations has recently been coordinated by the IPCC in conjunction with its Fourth Assessment Report (AR4). Many improvements in physics, numerical algorithms, and configurations have taken place in climate models since TAR, including newly developed treatments of subgrid parameterizations, widespread removal of flux adjustments, and generally increased resolution in both atmosphere and ocean as well as sea ice. Specifically, more sophisticated state-of-the-art sea ice thermodynamics and dynamics (e.g., Hibler 1979; Hunke and Dukowicz 1997; Bitz and Lipscomb 1999; Bitz et al. 2001) have become widely implemented in climate models. Rotated coordinates or curvilinear coordinates are now employed by many models to eliminate the polar singularity in ocean and sea ice models (e.g., Madec and Imbard 1996; Murray 1996). These model enhancements have the potential to reduce the uncertainties in the climate change projections. As part of the IPCC's coordinated international effort, we have analyzed sea ice simulations in the IPCC AR4 climate models forced by the observed and projected emissions forcings in the twentieth century and twenty-first century, evaluated the models' ability to capture the sea ice climate of the twentieth century, and assessed sea ice projections for the twenty-first century under the prescribed global warming scenarios.

2. Datasets

This study uses the gridded field of sea ice concentration over the Northern Hemisphere, including the Arctic Ocean and the adjacent marginal seas, from the participating climate models for the IPCC AR4. The various modeling centers participating with IPCC AR4 activity performed simulations of the climate of the twentieth century (20C3M) with observed anthropogenic or natural forcing. The coordinated suite of simulations was then extended to conduct runs under the prescribed IPCC SRES (Nakicenovic and Swart 2000) A1B, A2, and B1 scenarios. A committed climate change experiment called COMMIT that freezes greenhouse gas concentrations at levels observed in the year 2000 was also run through the year 2100. Most modeling centers performed multimember ensembles of simulations for each scenario, although the number of ensemble members varies among the models and scenarios. The outputs from all the models and scenarios were archived by the Program for Climate Model Diagnosis and Intercomparison (PCMDI; http://www-pcmdi.llnl.gov/about/index.php) at the Lawrence Livermore National Laboratory.

We analyzed the sea ice output from the abovementioned five simulation groups. Because of availability of sea ice concentration datasets on the PCMDI data server as of the IPCC deadline for model syntheses, our analysis covers various numbers of the IPCC AR4 models in the different simulation groups. We utilized outputs from 15 models for the 20C3M, 13 models for the SRES A1B and B1, 9 models for the SRES A2, and 10 models for the COMMIT. Because the various climate models differ in their formulations of physical processes in the atmosphere, ocean, and sea ice components, the simulations are obviously model dependent. In addition, the models have different resolutions and coupling strategies. Table 1 lists these models and provides a brief summary of their key characteristics. (Detailed information can be found online at http://www-pcmdi.llnl.gov/ipcc/model_documentation/ipcc_model_documentation.php and the embedded modeling centers' Web site links.)

3. Results

a. Sea ice climatology in the twentieth century

The climate of the twentieth century was simulated with the observed emissions forcing, including greenhouse gas concentrations and, in some cases, aerosol and variable solar forcing. To avoid potential impacts from model spinup, all the models were initialized at various antecedent times early in the mid- or late nineteenth century (Table 1). The models were integrated until the end of the twentieth century. We calculated sea ice areas for all the models in 20C3M listed in Table 1 over the Northern Hemisphere for their entire integration period. If more than one ensemble member was available for the particular model and scenario, our calculated areas are averaged over the ensemble members. To validate the models' simulation of Arctic sea ice cover, we used the observational analysis dataset

TABLE 1. Summary information about the IPCC AR4 models used in this study.

Model ID	Country	Realization		Initial time	Sea ice physics	Flux adjustment	Sea ice resolution	Natural forcing in 20C3M
CGCM3.1 (T47)	Canada	20C3M:	1	1850	• Energy balance • Cavitating fluid	Heat and water	1.85° × 1.85° 0 layers	No
		SRES A1B:	1					
		SRES A2:	1					
		SRES B1:	1					
		COMMIT:	1					
CNRM-CM3	France	20C3M:	1	1860	• Energy balance • Thickness distribution • Elastic–viscous–plastic rheology	None	2.0° × 2.0° 4 layers	No
		SRES A1B:	1					
		SRES A2:	1					
		SRES B1:	1					
		COMMIT:	1					
CSIRO-Mk3.0	Australia	20C3M:	1	1871	• Energy balance • Cavitating fluid	None	1.875° × 1.875° 1–2 layers	No
		SRES A1B:	1					
		SRES A2:	1					
		SRES B1:	1					
		COMMIT:						
GISS-AOM	United States	20C3M:	2	1850	• Energy balance • Cavitating fluid	None	4.0° × 3.0° 2 mass layers 4 thermal layers	No
		SRES A1B:	2					
		SRES A2:						
		SRES B1:	2					
		COMMIT:						
GISS-ER	United States	20C3M:	9	1880	• Energy balance • Viscous–plastic rheology	None	4.0° × 5.0° 4 layers	Yes
		SRES A1B:	5					
		SRES A2:	1					
		SRES B1:	1					
		COMMIT:	1					
FGOALS-g1.0	China	20C3M:	3	1850	• Energy balance • Thickness distribution • Elastic–viscous–plastic rheology	None	1.0° × 1.0° 16 layers	No
		SRES A1B:	3					
		SRES A2:						
		SRES B1:	3					
		COMMIT:	3					
INM-CM3.0	Russia	20C3M:	1	1871	• Energy balance • Thickness distribution • No dynamics	Water flux in the GIN, * Barents, and Kara Seas	2.5° × 2.0° 0 layers	Yes
		SRES A1B:	1					
		SRES A2:	1					
		SRES B1:	1					
		COMMIT:	1					
IPSL-CM4	France	20C3M:	1	1860	• Energy balance • Viscous–plastic rheology	None	2.0° × 2.0 ° cos(lat) 2 layers	No
		SRES A1B:	1					
		SRES A2:	1					
		SRES B1:	1					
		COMMIT:	1					

TABLE 1. *(Continued)*

Model ID	Country	Realization		Initial time	Sea ice physics	Flux adjustment	Sea ice resolution	Natural forcing in 20C3M
MIROC3.2(hires)	Japan	20C3M: SRES A1B: SRES A2: SRES B1: COMMIT:	1 1 1 	1900	• Energy balance • Elastic–viscous–plastic rheology	None	0.281 25° × 0.1875° 0 layers	Yes
MIROC3.2(medres)	Japan	20C3M: SRES A1B: SRES A2: SRES B1: COMMIT:	3 3 3 3 1	1850	• Energy balance • Elastic–viscous–plastic rheology	None	1.4° × 1.4° 0 layers	Yes
MRI-CGCM 2.3.2	Japan	20C3M: SRES A1B: SRES A2: SRES B1: COMMIT:	5 5 5 5 1	1851	• Energy balance • Drifting by ocean currents	Heat and salt fluxes	2.5° × 2.0° 0 layers	Yes
CCSM3	United States	20C3M: SRES A1B: SRES A2: SRES B1: COMMIT:	1 1 1 	1870	• Energy balance • Thickness distribution • Elastic–viscous–plastic rheology	None	g×1v3 (about 1.0°) 4 layers	Yes
PCM	United States	20C3M: SRES A1B: SRES A2: SRES B1: COMMIT:	2 1	1890	• Energy balance • Elastic–viscous–plastic rheology	None	27 km 4 layers	Yes
UKMO HadCM3	United Kingdom	20C3M: SRES A1B: SRES A2: SRES B1: COMMIT:	2 1 1 1 1	1860	• Energy balance • Drifting by ocean currents	None	1.25° × 1.25° 0 layers	No
UKMO HadGEM1	United Kingdom	20C3M: SRES A1B: SRES A2: SRES B1: COMMIT:	1 	1860	• Energy balance • Thickness distribution • Elastic–viscous–plastic rheology	None	1.0° × 1.0° 0 layers	Yes

* GIN Seas: Greenland–Iceland–Norwegian Seas.

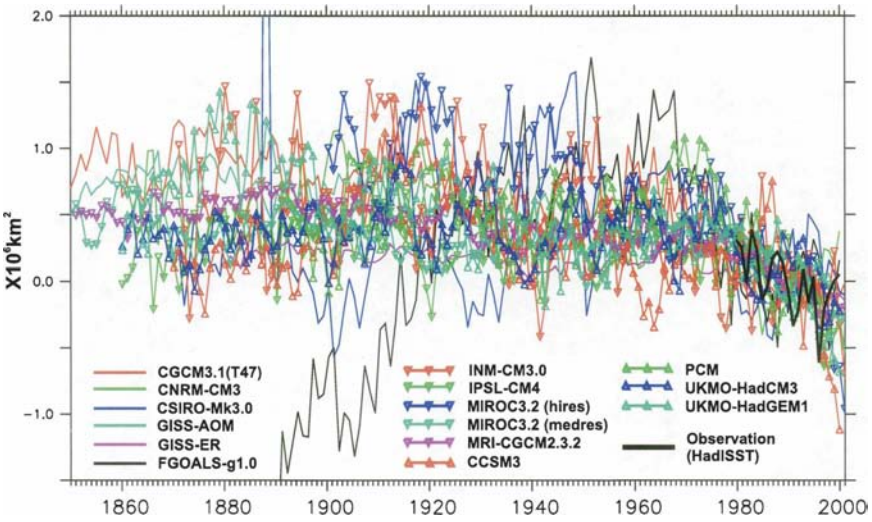

FIG. 1. Multimodel simulated annual mean sea ice area anomalies over the Northern Hemisphere in the 20C3M from 1850 to 2000. Plotted values are departures from 1979–99 climatological mean.

from the Hadley Centre Sea Ice and SST dataset (HadISST1; Rayner et al. 2003). This dataset consists of monthly $1° \times 1°$ gridded fields of sea surface temperature and sea ice concentration. Taking into consideration the accuracy of sea ice measurements in the real world we selected as a reference period 1979–99, years for which satellite remote sensing data were continuously available. Because a number of IPCC AR4 model runs finish in the year 1999, we did not include the year 2000 in the reference period.

Figure 1 shows the annual mean sea ice area from the ensemble mean of each IPCC AR4 model in the 20C3M simulations, in which the model integrations start from various years between 1850 and 1900 and end in 1999 or 2000; the climatological sea ice area during 1979–99 in each model has been removed. The time series contain interannual variability of various amplitudes. The Model for Interdisciplinary Research on Climate version 3.2 (MIROC 3.2) [high resolution (hires)] and Institute of Numerical Mathematics-Coupled Model version 3.0 (INM-CM3.0) show the largest fluctuations, while the Meteorological Research Institute-Global Coupled Atmosphere–Ocean General Circulation Model version 2.3.2 (MRI-CGCM2.3.2) exhibits the smallest variations from year to year. We examined the individual ensemble members of the MRI-CGCM2.3.2 and found that the annual mean sea ice area does not fluctuate consistently from year to year (not shown). Opposite amplitudes occur from time to time among the five members. Therefore, the large number of ensemble members may damp out interannual fluctuations. The Flexible Global Ocean–Atmosphere–Land System Model gridpoint version 1.0 (FGOALS-g1.0) demonstrates a rapid increase of sea ice area anomalies from 1850 to 1920 as an apparent spinup problem. Note that the large negative anomaly in FGOALS-g1.0 before 1920 does not mean that this model underestimates sea ice cover. Actually, this model starts from a much higher initial sea ice cover than do other models (not shown) and its follow-up increases lead to an excessively high sea ice cover (see next section). The time series of most other models' sea ice areas anomalies converge to a narrow band of fluctuations, particularly after the mid-1960s.

Sea ice change and variability in the models depend strongly on the simulated climatological state of the ice. Excessively small sea ice cover is more vulnerable to melting away in global warming scenarios. Therefore, a model with underestimated climatological sea ice coverage could be more sensitive to increases of emissions forcing. We quantified the climatological annual mean sea ice area during 1979–99 in the models and made a comparison with the observational analysis dataset HadISST1 (Fig. 2a). The HadISST1 data show an annual mean sea ice area over the Northern Hemisphere of 1.06×10^7 km^2. Most of the models captured this value well, within a range of 20.0%, except FGOALS-g1.0, which vastly overestimated the sea ice cover (Table 2). Specifically, the third-generation Coupled Global Climate Model (T47 version) [CGCM3.1(T47)], Goddard Institute for Space Studies-Atmosphere–Ocean Model (GISS-AOM), Institut Pierre Simon Laplace Coupled Model version 4 (IPSL-CM4), MIROC3.2 [medium resolution (medres)], Community Climate System Model version 3.0 (CCSM3), and the Met Office (MO; formerly UKMO) Third Hadley Cen-

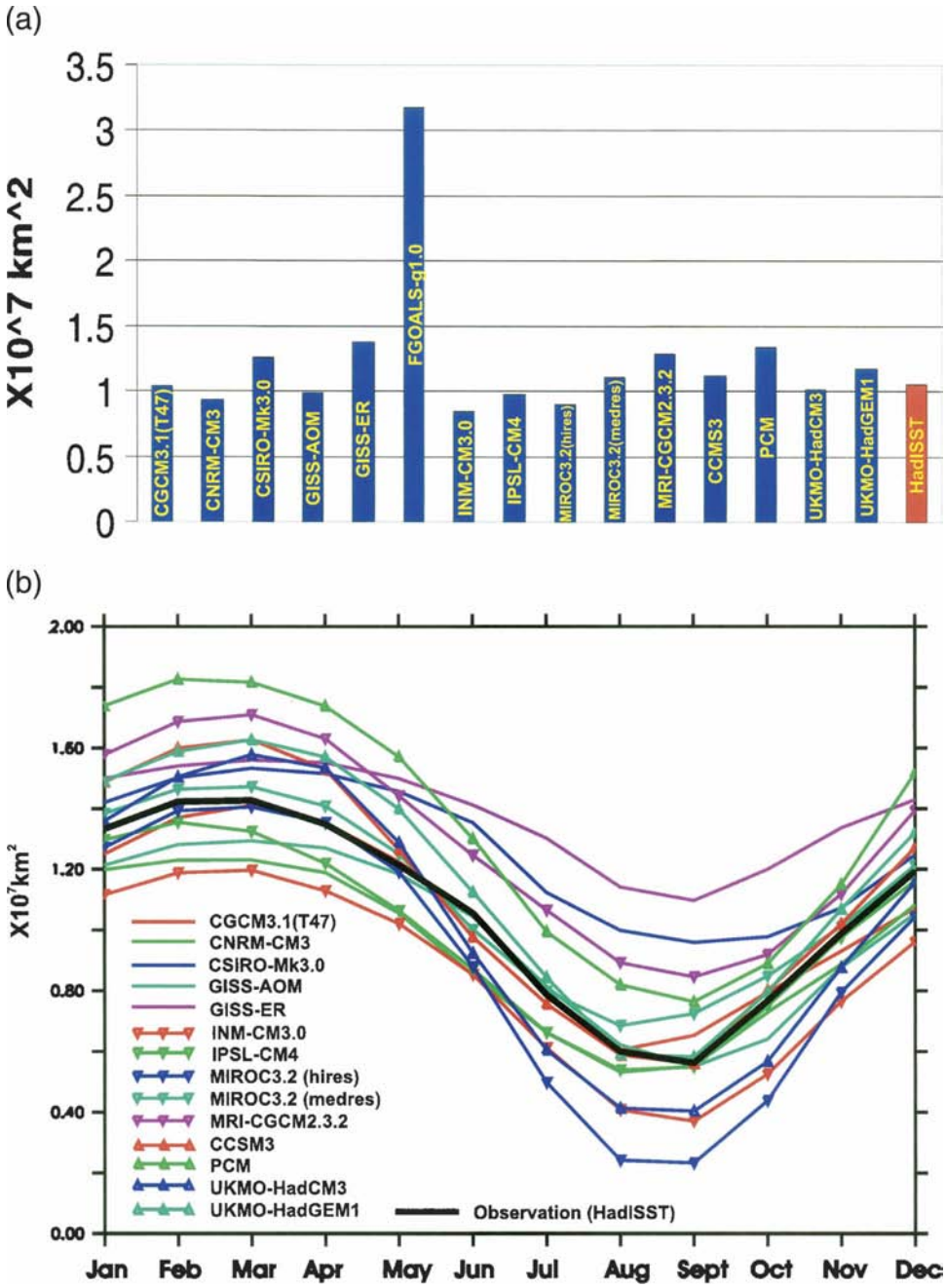

FIG. 2. Climatological (a) annual mean and (b) seasonal cycles of sea ice areas during 1979–99 over the Northern Hemisphere from 15 IPCC AR4 models in the 20C3M simulations and from the HadISST1 observational analysis data.

tre Coupled Ocean–Atmosphere GCM (HadCM3) models show errors of less than 10.0% relative to the observational climatology. The multimodel ensemble mean (excluding FGOALS-g1.0) climatological annual mean sea ice area is about 1.10×10^7 km^2, very close to the observational value.

Sea ice coverage displays a large seasonal cycle, reaching a maximum area of 14.3×10^7 km^2 in March and a minimum area of 5.6×10^7 km^2 in September according to observations from 1979 to 1999. The IPCC AR4 models generally capture the main characteristics of this seasonal course (Fig. 2b). However, apparent differences exist relative to the observations, either as overestimated or underestimated sea ice cover throughout the whole year or as an overestimated seasonal cycle amplitude. For example, the Commonwealth Sci-

TABLE 2. Summary statistics of sea ice area over the Northern Hemisphere during 1979–99, including the annual mean sea ice area in $\times 10^7$ km^2 and its difference from observations in percent (in parentheses); standard deviation of modeled seasonal cycle relative to observations in $\times 10^6$ km^2; linear trends in $\times 10^5$ km^2 decade^{-1} and in % decade^{-1} (in parentheses); multimodel ensemble mean and crossing-model standard deviation of the linear trends in $\times 10^5$ km^2 decade^{-1} and in % decade^{-1} (in parentheses).

Model ID	Annual mean	Std dev	Trend
CGCM3.1 (T47)	1.04 (−1.9)	0.58	−1.06 (−1.01)
CNRM-CM3	0.93 (−12.3)	1.44	0.40 (0.43)
CSIRO-Mk3.0	1.26 (18.9)	2.50	2.26 (1.82)
GISS-AOM	0.99 (−6.6)	0.99	−1.86 (−1.85)
GISS-ER	1.38 (30.2)	3.72	−0.57 (−0.41)
FGOALS-g1.0	3.17 (199.1)	22.33	−0.41 (−0.13)
INM-CM3.0	0.85 (−19.8)	2.23	−1.49 (−1.73)
IPSL-CM4	0.98 (−7.5)	1.00	−3.92 (−3.84)
MIROC3.2 (hires)	0.90 (−15.1)	2.18	−3.15 (−3.39)
MIROC3.2 (medres)	1.11 (4.7)	0.71	−1.47 (−1.31)
MRI-CGCM2.3.2	1.29 (21.7)	2.52	−2.30 (−1.75)
CCSM3	1.12 (5.7)	1.15	−6.16 (−5.20)
PCM	1.34 (26.4)	3.16	−3.36 (−2.44)
UKMO HadCM3	1.02 (-3.8)	1.46	−1.44 (−1.40)
UKMO HadGEM1	1.17 (10.4)	1.38	−5.10 (−4.19)
Observation (HadISST)	1.06	—	−2.05 (−1.90)
Multimodel ensemble mean*	1.10	1.79	−2.09 ± 2.17 (−1.88 ± 1.87)

* The model FGOALS-g1.0 is excluded.

entific and Industrial Research Organization-Mark 3.0 (CSIRO-Mk3.0), GISS-Model E–Russell (ER), MRI-CGCM2.3.2, and Parallel Climate Model (PCM) models apparently produce greater sea ice areas during the entire 12 months, while the INM-CM3.0 and MIROC3.2(hires) models produce a smaller sea ice area. The MO HadCM3 model shows an enlarged seasonal fluctuation, with an overestimated sea ice area in winter but an underestimated sea ice area in summer. Overall, the CGCM3.1(T47), Centre National de Recherches Meteorologiques Coupled Global Climate Model version 3 (CNRM-CM3), GISS-AOM, IPSL CM4, MIROC3.2(medres), CCSM3, MO HadCM3, and MO Hadley Centre Global Environmental Model version 1 (HadGEM1) show relatively small errors in comparison with observations, with standard deviations relative to observational climatology of smaller than 2.0 $\times 10^6$ km^2 (Table 2). Preliminary examination based on the available data indicates no readily identifiable relationship between the models' seasonal cycle simulation and model physics or configuration. Results from the FGOALS-g1.0 model are not shown in Fig. 2b because of that model's excessive ice cover. Considering that FGOALS-g1.0 has very serious problems shown above in reproducing present climate and hence does not represent the state of the art of climate models, we excluded this model from the following analyses.

Most IPCC AR4 models also show consistency with observations in reproducing the decreasing trend of sea ice area during 1979–99 (Fig. 1 and Table 2). Exceptions are CNRM-CM3 and CSIRO-Mk3.0, which show increases. Pronounced shrinkage of Arctic sea ice coverage in the recent 20–30 yr has been documented (e.g., Parkinson et al. 1999; Parkinson and Cavalieri 2002; Cavalieri and Parkinson 2003). A least squares linear fit to the satellite passive microwave data gives a decreasing trend in the Northern Hemisphere sea ice extent of -3.29×10^5 km^2 decade^{-1} or −2.7% decade^{-1} over the period 1979–99 (Parkinson and Cavalieri 2002). The reduction of Arctic sea ice coverage has accelerated in the most recent years, leading to record minima of the Arctic summer sea ice extent in 2002 and 2004 (Serreze et al. 2003; Stroeve et al. 2005).

The sea ice reduction can be attributable to both greenhouse warming (e.g., Vinnikov et al. 1999) and to natural variability represented by the North Atlantic Oscillation (NAO) or the Arctic Oscillation (AO; e.g., Thompson and Wallace 1998; Zhang et al. 2003). The impact of the AO on sea ice changes was isolated by a modeling study (Zhang et al. 2003), which showed that the total sea ice cover pronouncedly decreases in the AO's positive phase. In particular, the sea ice cover in the Eurasian shelf seas has undergone a large reduction because of the spread of warmer temperature from the Eurasian continent into the ocean. The recent large decrease of sea ice cover from the late 1980s to the mid-1990s, when the NAO/AO persists in its positive phase with large amplitude (Thompson and Wallace 1998), can be accounted for by this mechanism to a large degree. Furthermore, the anthropogenic forcing

and the NAO/AO may not be independent. If the anthropogenic forcing leads to an increase in frequency of the positive phase and amplitude of NAO/AO, the NAO/AO would strengthen the anthropogenic forcing on sea ice decrease. The relative impacts of the anthropogenic forcing and the NAO/AO on sea ice retreat, and the impacts of the anthropogenic forcing on the NAO/AO, have not been well clarified.

Many observational studies have been based on sea ice extent, which is more reliably estimated than ice area from satellites. However, taking advantage of the climate models' output of sea ice concentrations, we used sea ice area in this study in order to permit inclusion of the effects of ice-free area, such as leads and polynyas. Unlike ice extent, the calculation of sea ice area does not require a threshold of sea ice concentration. Sea ice area is usually smaller than sea ice extent for the entire Arctic domain. The HadISST1 data indicate a linear decreasing trend of -2.05×10^5 km^2 decade^{-1} or -1.90% decade^{-1} of Northern Hemisphere sea ice area over the period 1979–99 (Table 2). The decreasing trends in the IPCC AR4 models range from -0.57×10^5 km^2 decade^{-1} or -0.41% decade^{-1} in GISS-ER to -6.16×10^5 km^2 decade^{-1} or -5.2% decade^{-1} in CCSM3. These differing rates of decrease generally correspond to the overall surface air temperature increases in the respective models (Wang et al. 2005, manuscript submitted to *J. Climate*, hereafter WAN).

In contrast to observations and most models, CNRM-CM3 and CSIRO-Mk3.0 show positive trends during 1979–99, though the mean value in this period is obviously lower than in earlier periods. In these two models, the sea ice areas in 1979–99 are mainly modulated by interannual variability. The increasing trends can be accounted for by the decrease of surface air temperatures simulated by these two models during the same period (WAN). As discussed above, changes of sea ice, as well as surface air temperature, are impacted by both the anthropogenic forcing and natural variability. During the recent several decades, the greenhouse gas concentration increased (Nakicenovic and Swart 2000). The observed sea ice cover decrease and surface air temperature increase should be reflections of this anthropogenic forcing. Natural variability is superimposed on the long-term trends to influence the timing and magnitude of sea ice area trends. However, the observations and simulation results from most models indicate that the anthropogenically forced sea ice decrease predominates over the natural variability. In this sense, the inconsistency between the CNRM-CM3 and CSIRO-Mk3.0 simulations and the observations suggests that these two models do not capture sea ice changes well, at least in magnitude, forced by the anthropogenic forcing. Furthermore, the NAO/AO has been identified as a leading mode representing natural variability, which contributed to the sea ice decrease in the 1990s. Although there is no reason that the model and observed trends should "line up" in time if the changes of sea ice are instead part of the natural variability, the opposite changes of sea ice area in CNRM-CM3 and CSIRO-Mk3.0 are contrary to observations, indicating that these two models are not consistent with the actual phase and amplitude changes of the NAO/AO.

The use of a multimodel ensemble mean can add robustness to an estimate of a trend of sea ice coverage. In this case, the multimodel ensemble mean trend is -2.09×10^5 km^2 decade^{-1} or -1.88% decade^{-1} (Table 2), which is very close to the observational estimate. However, the large across-model standard deviation of the model estimates relative to observation points to obvious model-dependent uncertainties.

Additionally, though three IPCC AR4 models [CGCM3.1(T47), INM-CM3.0, and MRI-CGCM2.3.2] use flux adjustment for water and/or heat (Table1), they do not show an overall improvement over those models without flux adjustment in simulating the climatological annual mean, seasonal cycle, and decreasing trends of sea ice areas. For example, the multimodel ensemble mean of climatological annual mean sea ice area and seasonal cycle standard deviation for the models are very similar with and without flux adjustment, with the annual mean areas of 1.01×10^7 km^2 and 1.06×10^7 km^2 and standard deviations of 1.79×10^6 km^2 and 1.78×10^6 km^2, respectively. The multimodel ensemble mean for the models without flux adjustment exhibits a more observationally consistent estimate of decreasing trend of -2.07×10^5 km^2 decade^{-1} than the estimate of -1.62×10^5 km^2 decade^{-1} produced by models with flux adjustment. This suggests that implementation of sophisticated treatments of model physics might lead to improvements of sea ice simulations in climate models, since the three models with flux adjustment generally use a relatively simple treatment of sea ice physics compared to other models (Table 1). However, because sea ice has complex interactions with the atmosphere and ocean, the attributions of sea ice simulation problems can hardly be made without a carefully designed set of controlled experiments.

b. *Accelerated sea ice area reductions in the SRES scenarios*

Emissions forcing may remain high and could be even further enhanced in the twenty-first century, leading to a continuation and intensification of global warming and sea ice coverage reduction over the Arc-

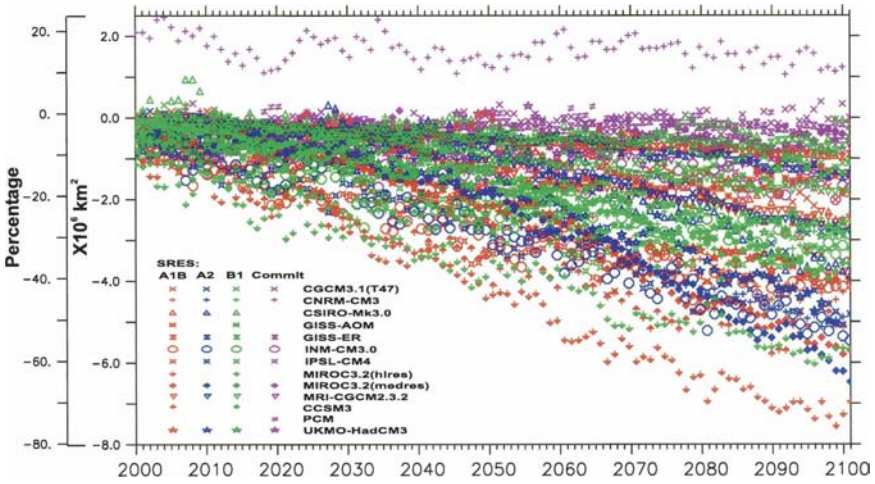

FIG. 3. Projections of annual mean sea ice area anomalies over the Northern Hemisphere from 2000 to 2100, relative to the 1979–99 climatologies. The areal anomalies are the difference between each model's simulated ice area and the 1979–99 climatological mean of the same model. The corresponding percentage changes, adjusted for biases in the models' 1979–99 climatologies, are also shown.

tic. The SRES A1B, A2, and B1 scenarios of emissions forcing were recommended for modeling experiments for the IPCC AR4. These three scenarios can be characterized by unmitigated emissions leading to an increase of atmospheric CO_2 concentrations to over 800 ppm in A2, and constrained emissions leading to increases to 770 ppm in A1B and 550 ppm in B1 by the end of 2100, up from 368 ppm in 2000 (IPCC 2001). More details can be found in IPCC reports (Nakicenovic and Swart 2000; IPCC 2001; Houghton et al. 2001). Additional parallel "committed" climate change simulations (COMMIT) were also conducted, in which the emissions forcing is kept at the level of the year 2000.

The responses of sea ice area in the IPCC AR4 models to the emissions forcing under SRES A1B, A2, and B1 as well as COMMIT demonstrate marked diversity, ranging from an accelerated decreasing trend to a nearly constant level (Fig. 3), superimposed on which are apparent interannual- and decadal-scale variability. In comparison with the decrease during 1979–99, the decreases of sea ice area are generally intensified in the SRES scenarios over the entire twenty-first century, although a few models show very flat slopes (Table 3). The MIROC3.2(hires) and GISS-ER models are the two extreme examples, showing the largest and smallest sea ice reductions. In the climatological simulations discussed in the preceding section, the MIROC3.2(hires) (GISS-ER) model considerably underestimated (overestimated) annual mean sea ice area and overestimated (underestimated) sea ice area decreasing trends (Table 2). It is intuitive to examine whether the ability of sea ice area simulations in the twentieth century continues to impact the simulations in the twenty-first century. A scatterplot of annual mean sea ice area during 1979–99 (representing initial status of sea ice) and the rates of decrease of the annual mean sea ice area in the twenty-first century in the SRES A1B, A2, and B1 scenarios was made (not shown). The results show a general negative correlation, indicating that the initial sea ice simulation condition is a factor to influence the projection of sea ice changes; a smaller initial sea ice area giving rise to a larger reduction of sea ice area. However, this negative correlation is sensitive to the models involved in the calculation, which, for example, can be negligible in the SRES A1B and A2 if the GISS-ER model is excluded. Under the same global warming scenario, the simulated physical feedbacks related to surface albedo, cloud, and so on can be quite different depending on the model. These differences result in varied increases in surface heat budgets, which is important in the sea ice change projection simulations and complicates the relationships such as initial sea ice area and sea ice area reduction rate discussed above. In addition, the decreasing trends of sea ice in GISS-ER and CCSM3 are weakened in the twenty-first century compared to 1979–99.

In the COMMIT simulations, most models do not show obvious linear trends of sea ice decrease. Only a few models show weaker decreasing trends than those observed during the period 1979–99. A slight increase occurs in the CGCM3.1(T47) simulations. Comparisons of sea ice area changes among SRES A1B, A2, and B1 and COMMIT suggest that an increase of emissions forcing results in a readily apparent shrinkage of sea ice

TABLE 3. The IPCC AR4 model-projected linear trends of the annual mean sea ice area over the Northern Hemisphere from 2000 to 2100. The trends are shown here in $\times 10^5$ km^2 decade^{-1} and in % decade^{-1} (in parentheses). The "+" and "−" signs (in parentheses), respectively, denote strengthened and weakened rates of sea ice retreat compared to those during the period 1979–99. The multimodel ensemble means and crossing-model standard deviations are also given in the right bottom row in $\times 10^5$ km^2 decade^{-1} and in % decade^{-1} (in parentheses). The bold fonts indicate that the corresponding model-estimated trend falls within the 99% confidence interval.

Model ID	Trends		
	SRES A1B	SRES A2	SRES B1
CGCM3.1 (T47)	−1.95 (−1.87) (+)	**−3.08** (−2.96) (+)	−1.09 (−1.04) (+)
CNRM-CM3	**−4.45** (−4.77) (+)	**−5.10** (−5.46) (+)	**−2.62** (−2.81) (+)
CSIRO-Mk3.0	**−3.02** (−2.39) (+)	**−4.43** (−3.51) (+)	−0.91 (−0.72) (+)
GISS-AOM	−1.24 (−1.26) (−)	—	−0.94 (−0.95) (−)
GISS-ER	−1.16 (−0.84) (+)	−1.62 (−1.17) (+)	−0.69 (−0.50) (+)
INM-CM3.0	**−2.94** (−3.48) (+)	**−3.92** (−4.64) (+)	**−2.13** (−2.52) (+)
IPSL-CM4	**−3.05** (−3.10) (−)	**−4.02** (−4.09) (+)	**−2.75** (−2.80) (−)
MIROC3.2 (hires)	−5.87 (−6.56) (+)	—	−3.96 (−4.42) (+)
MIROC3.2 (medres)	−6.11 (−5.52) (+)	−6.44 (−5.83) (+)	−3.88 (−3.51) (+)
MRI-CGCM2.3.2	**−3.48** (−2.69) (+)	**−3.70** (−2.86) (+)	**−2.50** (−1.93) (+)
CCSM3	−5.28 (−4.70) (−)	—	**−2.46** (−2.19) (−)
UKMO HadCM3	**−3.91** (−3.84) (+)	**−4.38** (−4.30) (+)	**−2.78** (−2.73) (+)
Multimodel ensemble mean	−3.54 ± 1.66 (−3.42 ± 1.74)	−4.08 ± 1.33 (−3.87 ± 1.43)	−2.22 ± 1.11 (−2.18 ± 1.20)

area, along with a surface air temperature rise. The greater the emissions forcing, the more rapid the decrease in sea ice area. The increased sea ice area reductions under the SRES scenarios correspond well to overall surface air temperature increases (ACIA 2005).

The overall changes of sea ice area projected for 2000–2100 are quantified in Table 3. The linear trends vary among models and among scenarios, ranging from -0.69×10^5 km^2 decade^{-1} or −0.50% decade^{-1} in GISS-ER in SRES B1 to -6.44×10^7 km^2 decade^{-1} or −5.51% decade^{-1} in MIROC3.2(medres) in SRES A2. Overlaps of the sea ice area evolution across different scenarios are obvious. Large uncertainties accordingly emerge in the sea ice change projections. Nonetheless, comparison of the decreasing trends among the three scenarios indicates that changes of sea ice areas are generally most conservative in SRES B1, for which the rates of decrease are generally smallest. By contrast, sea ice area is most vulnerable in SRES A2, for which the rates of decrease are largest, coinciding with the projected changes of surface air temperatures in the corresponding models and scenarios (Chapman and Walsh 2005, manuscript submitted to *J. Climate*, hereafter CW). The multimodel ensemble mean rates of sea ice area decease are $-3.54 \pm 1.66 \times 10^5$ km^2 decade^{-1} or −3.42% ± 1.74% decade^{-1} for the A1B scenario, $-4.08 \pm 1.33 \times 10^5$ km^2 decade^{-1} or −3.87% ± 1.43% decade^{-1} for the A2 scenario, and $-2.22 \pm 1.11 \times 10^5$ km^2 decade^{-1} or −2.18% ± 1.20% decade^{-1} for the B1 scenario. As a consequence, the annual mean sea ice areas during the last 20 yr of the twenty-first century (2080–2100) under the A1B, A2, and B1 scenarios are reduced to 0.74×10^7 km^2, 0.73×10^7 km^2, and 0.84×10^7 km^2, equivalent to changes of −31.09%, −33.39%, and −21.55% relative to observed area during the period of 1979–99.

The relatively large standard deviations shown in Table 3 quantitatively reinforce the across-model scatter shown in Fig. 3. We assumed the models' estimates of sea ice changes shown in Table 3 are members of a sample from a population. We performed a statistical error analysis by introducing the confidence interval to objectively define ranges within which real mean trends of sea ice changes would fall, and to quantify the amount of uncertainty or error involved in the projected changes of sea ice area by the various climate models. The confidence interval (CI) for the mean, which also measures the degree to which the sampled data are consistent, is defined as follows (Lane 2002):

$$\mathrm{CI} = \overline{X} \pm t \times S, \tag{1}$$

where $\overline{X}$ is the sample mean, t is the Student's t distribution, and S is the standard error, which is calculated by $S = \sigma/\sqrt{n}$. The standard deviation is denoted by σ and n is the sample size.

Statistical computation gives 99% confidence intervals from -5.03 to -2.05×10^5 km^2 decade^{-1} for SRES A1B, from -5.57 to -2.59×10^5 km^2 decade^{-1} for A2, and -3.09 to -1.35×10^5 km^2 decade^{-1} for B1. This implies, based on the participating models in this study (recall it is assumed statistically to be a sample of a population), that one can have 99% confidence that real mean values of sea ice change would fall into these ranges in the respective scenarios. A substantial subset

of the models (almost the same in all three scenarios) falls into these 99% confidence intervals (see bold fonts in Table 3), indicating a great degree of consistency in projecting sea ice area changes, not only within each scenario but also across all three scenarios, with decreasing trends. The trends that fall outside of the confidence interval are due to either extremely small (e.g., in GISS-AOM and GISS-ER) or extremely large [e.g., in MIROC3.2(hires) and MIROC3.2(medres)] estimates.

The width of the intervals is a quantitative representation of uncertainties in the estimates of sea ice area changes. In spite of the consistency among many of the IPCC AR4 models in the projection of sea ice area changes, we still find wide confidence intervals, implying a large amount of uncertainty. We examined potential influence of the "natural variability" on the simulated trends. We selected the A1B scenario simulations by the GISS-ER and MRI-CGCM2.3.2 models, which have the largest number of ensemble members (five members in each model) among all IPCC AR4 model simulations. Large differences of variability obviously occur among the ensemble members in both of these models, with different phases and amplitudes (not shown). However, all members show similar decreasing trends, which range from -1.04 to -1.26×10^5 km^2 decade^{-1} in GISS-ER and from -3.14 to -3.68×10^5 km^2 decade^{-1} in MRI-CGCM2.3.2. The across–ensemble member standard deviations are 0.10×10^5 km^2 decade^{-1} in GISS-ER and 0.22×10^5 km^2 decade^{-1} in MRI-CGCM2.3.2, respectively, which are considerably smaller than the across-model standard deviation of 1.66×10^5 km^2 decade^{-1}. This suggests that the natural variability does not have a large influence on the trends in these two models.

We also examined the extreme estimates in the models. The extreme estimates in the aforementioned by the GISS-ER and MIROC3.2(hires) models do not differ from the mean trends by more than would be expected from the differences among these models' various simulations of the climate of the twentieth century, which show larger (smaller) mean sea ice areas and lower (higher) sea ice reduction rates than other models; extreme estimated values from other models might arise from complications of model physics as well as model sensitivity to emissions forcing. The specific causes for the large scatter among all models are not really identifiable based on the available information and data. To reduce the uncertainty, more simulations from more models (i.e., more sampling) and continued improvements of model physics are needed, together with diagnostic assessments of the reasons for the differing rates of sea ice retreat among the models.

c. *Contrasting changes of multiyear and seasonal ice in the SRES scenarios*

Sea ice can be decomposed to multiyear sea ice and seasonal ice over the Arctic Ocean. Multiyear ice, which is the major component of the Arctic Ocean's present ice cover, is ice that has survived at least one summer melt season. Disproportionate changes of multiyear and seasonal sea ice will definitely change air–sea interactions temporally and spatially and, in turn, impact the Arctic energy and water cycles. The multiyear sea ice is usually distinguished from the seasonal ice by its characteristics of greater thickness and higher albedo (e.g., Comiso 2002; Kwok 2004). In conjunction with the reduction of Arctic total sea ice in recent decades, a dramatic decline of multiyear sea ice from 1978 to 2000 has also been identified by Comiso (2002). State-of-the-art climate models do not explicitly separate the sea ice into multiyear ice and seasonal ice. They also do not provide accurate information about sea ice thermal and optical properties in order to distinguish multiyear ice from total sea ice outputs. Consequently, we follow Comiso's (2002) approach by using the summer minimum sea ice area as a proxy indicator of multiyear ice area. We accordingly define each year's seasonal ice (or first-year ice) area as the difference between the largest sea ice area and the multiyear sea ice area (summer minimum sea ice area) for that year. In this definition, the second-year ice is categorized as belonging to the multiyear sea ice.

Figure 4a shows the projected changes of multiyear ice area during the twenty-first century after subtraction of the climatological mean for the period of 1979–99. Like the total sea ice, the multiyear ice shows a large decrease in all IPCC AR4 models in all SRES scenarios. The multiyear sea ice area decreases faster than the total sea ice area. Generally, the decreasing rates in SRES A1B and A2 are greater than in B1. The COMMIT simulations yield the smallest multiyear sea ice reduction. Similar to the annual mean sea ice area, the multiyear sea ice areas do not show obvious declining trends in a number of models in the COMMIT simulations [e.g., CGCM3.1(T47) and GISS-ER]. A comparison of the rates of multiyear ice area decrease between SRES scenarios and COMMIT reinforces the emissions forcing's impacts on the intensification of sea ice loss.

The rates of multiyear sea ice area decrease diverge more rapidly than the annual mean sea ice area shown in Fig. 3. Two visible groups emerge: CGCM3.1 (T47), CSIRO-Mk3.0, GISS-AOM, GISS-ER, and MRI-CGCM2.3.2 show smaller ice reductions, while CNRM-CM3, INM-CM3.0, IPSL CM4, MIROC3.2(hires), MIROC3.2(medres), CCSM3, and MO HadCM3 show

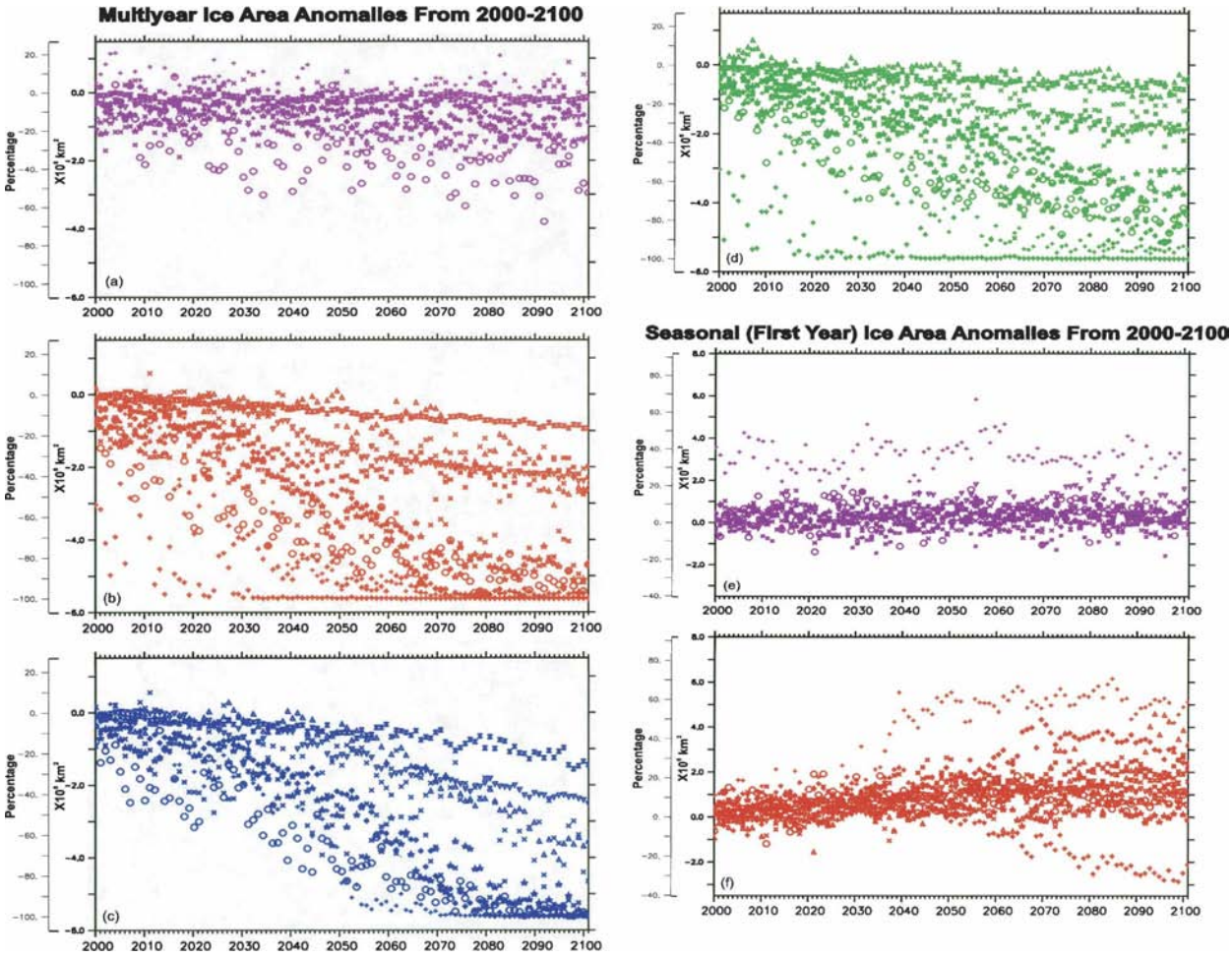

FIG. 4. The same as Fig. 3, but partitioned for (a) COMMIT, (b) A1B, (c) A2, and (d) B1 for multiyear sea ice area and (e) COMMIT, (f) A1B, (g) A2, and (h) B1 for seasonal ice area.

larger values. Specifically, the GISS-ER model estimates the smallest multiyear ice decrease, while the multiyear sea ice in the MIROC3.2(hires) model collapses rapidly to nearly zero before 2020 in both the SRES A1B and B1 (no available data for A2) and then maintains a low multiyear ice cover for the rest of the twenty-first century. The first ice-free Arctic Ocean occurs in the year 2062 as projected by this model. The models CNRM-CM3, INM-CM3.0, and CCSM3 also show very large decreases, with the multiyear ice reduced by over 80% in the second half of the twenty-first century; however, there is no ice-free ocean projected to occur in the twenty-first century in the simulations by these models.

In contrast to the changes of multiyear sea ice area, the seasonal ice area increases in almost all the models, as shown in Fig. 4b, from which the climatology during 1979–99 has again been removed. Taking into account the total ice area decreases shown in Fig. 3, a seasonal ice area increase implies that the total sea ice area shrinkage is mainly due to loss of multiyear ice. The changes of seasonal ice compensate for the multiyear sea ice loss to some degree, thereby reducing the rate of annual average sea ice loss. The persistent increases of seasonal ice area occur consistently in most IPCC AR4 models throughout the entire twenty-first century. Only a couple of models show different behavior, a decline after the middle of the twenty-first century after several decades' rise [e.g., MIROC3.2(hires)]. Compared with the annual and multiyear sea ice areas, the seasonal ice area changes in most models are constrained within a relatively narrow band. As an extreme case, the CNRM-CM3 model projects the largest positive anomalies of seasonal ice area in all three SRES scenarios compared with other models. The seasonal ice area rapidly increases from 2030 to 2050 and then

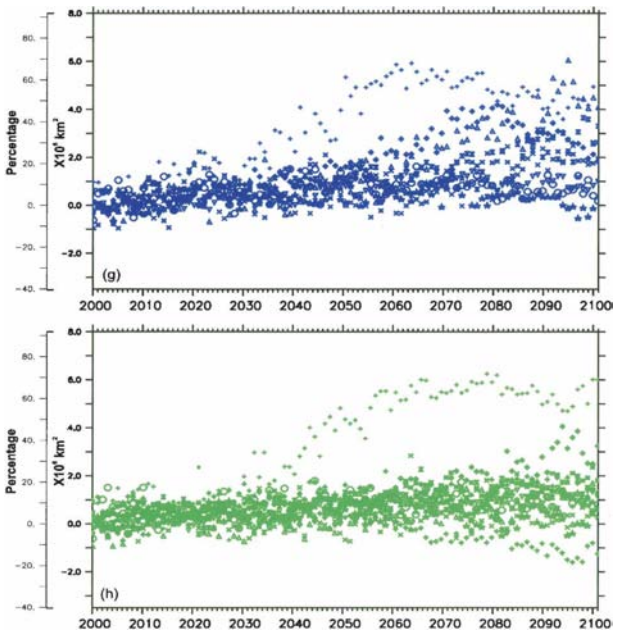

FIG. 4. (*Continued*)

maintains high values until the end of the century. Not surprisingly, this model has one of the largest rates of multiyear ice loss. The CSIRO-Mk3.0 and MIROC3.2(medres) are the other two models that show large increases of seasonal ice areas.

The long-term contrasting changes of multiyear and seasonal sea ice areas are quantified by the least squares method. The resultant linear trends seen between the multiyear and seasonal ice areas listed in Table 4 show a strong negative correlation among most IPCC AR4 models for all the three SRES scenarios, except for MIROC3.2(hires) and MO HadCM3, which show decreases in both the multiyear and seasonal ice areas. Generally, the largest decreases/increases of multiyear/seasonal ice areas occur in SRES A2, while the smallest values appear in B1. Specifically, the estimated trends of multiyear ice area range from -0.53×10^5 km^2 decade^{-1} or -2.30% decade^{-1} in MIROC3.2(hires) in B1 to -8.72×10^5 km^2 decade^{-1} or -12.72% decade^{-1} in MIROC3.2(medres) in A1B, and the changes of seasonal ice area vary from -5.40×10^5 km^2 decade^{-1} or -4.59% decade^{-1} in MIROC3.2(hires) in A1B to 5.25×10^5 km^2 decade^{-1} or 7.40% decade^{-1} in CNRM-CM3 in B1.

In addition, it is worthwhile to point out that the MIROC3.2(hires) and MIROC3.2(medres) models are the same model with different resolutions, but they produce completely different changes of seasonal ice. The former gives a change of -5.40×10^5 km^2 decade^{-1}, while the latter gives a change of 3.56×10^5 km^2 decade^{-1}, illustrating the impact of resolution on simulations. Actually, this impact already appeared in the simulation of the climate of the twentieth century. Comparisons of climatological means during 1979–99 indicate that the sea ice is considerably smaller in area and also thinner in MIROC3.2(hires) than in MIROC3.2(medres). Only a small area of sea ice appears north of the Greenland, with a thickness ranging from 0.2 to 0.6 m, in MIROC3.2(hires) in September.

TABLE 4. The IPCC AR4 model-projected linear trends of the multiyear sea ice area and seasonal ice area. The trends are shown here in $\times 10^5$ km^2 decade^{-1} and in % decade^{-1} (in parentheses). The multimodel ensemble means and crossing-model standard deviations are listed in the last row in $\times 10^5$ km^2 decade^{-1} and in % decade^{-1} (in parentheses). The bold fonts indicate that the corresponding model estimated trend falls within the 99% confidence intervals.

	Multiyear ice			Seasonal ice		
Model ID	SRES A1B	SRES A2	SRES B1	SRES A1B	SRES A2	SRES B1
CGCM3.1 (T47)	**−2.63** (−4.36)	**−4.15** (−6.86)	−1.29 (−2.13)	**1.07** (1.32)	**1.69** (2.09)	**0.19** (0.23)
CNRM-CM3	−6.18 (−11.70)	**−6.97** (−13.19)	−5.82 (−11.01)	4.64 (6.55)	4.50 (6.34)	5.25 (7.40)
CSIRO-Mk3.0	**−4.21** (−4.39)	**−6.45** (−6.72)	**−1.32** (−1.37)	**2.20** (3.82)	**3.36** (5.85)	**0.82** (1.43)
GISS-AOM	**−2.00** (−3.63)	—	**−1.51** (−2.74)	**1.92** (2.58)	—	**1.45** (1.95)
GISS-ER	−1.67 (−1.52)	−2.38 (−2.17)	−1.12 (−1.02)	**0.96** (2.07)	**1.34** (2.90)	**0.72** (1.56)
INM-CM3.0	**−2.61** (−7.06)	**−3.15** (−8.50)	**−2.28** (−6.15)	**0.26** (0.31)	**0.37** (0.45)	**0.51** (0.61)
IPSL-CM4	**−3.91** (−7.28)	**−4.90** (−9.11)	**−3.15** (−5.86)	**1.60** (1.96)	**2.08** (2.54)	**0.92** (1.12)
MIROC3.2 (hires)	−1.58 (−6.86)	—	−0.53 (−2.30)	−5.40 (−4.59)	—	−3.00 (−2.55)
MIROC3.2 (medres)	−8.72 (−12.72)	−8.27 (−12.07)	−5.59 (−8.16)	3.56 (4.52)	**3.28** (4.17)	**2.58** (3.28)
MRI-CGCM2.3.2	**−4.26** (−5.04)	**−4.19** (−4.96)	**−3.31** (−3.91)	**1.70** (1.96)	**1.26** (1.46)	**1.52** (1.76)
CCSM3	**−5.04** (−9.00)	—	**−3.59** (−6.41)	**1.12** (1.05)	—	**1.90** (1.78)
UKMO HadCM3	**−3.54** (−8.78)	**−4.00** (−9.92)	**−2.55** (−6.33)	**−0.39** (−0.33)	0.06 (0.05)	**−0.30** (−0.26)
Multimodel ensemble mean	−3.86 ± 2.07	−4.94 ± 1.91	−2.67 ± 1.71	1.10 ± 2.46	1.99 ± 1.47	1.05 ± 1.92
	[−4.19 ± 2.13]*	(−8.17 ± 3.44)	[−2.94 ± 1.76]*	[1.73 ± 1.57]*	(2.87 ± 2.21)	[1.36 ± 1.67]*
	(−6.86 ± 3.32)		(−4.78 ± 3.05)	(1.77 ± 2.75)		(1.52 ± 2.34)

* Trends and std devs using the same models as SRES A2.

The significantly underestimated sea ice was used as the initial condition for the SRES scenario simulations. As a consequence, sea ice cannot survive for long in summer in the SRES scenario simulations. An ice-free summer results in a strongly warmed ocean and atmosphere, which leads to a decrease of seasonal ice production subsequently. The reason for this bias in the sea ice simulations for the climate of the twentieth century has not been identified.

The multimodel ensemble mean shows a multiyear ice area change of -3.86×10^5 km^2 decade^{-1} or -6.86% decade^{-1} in A1B, -4.94×10^5 km^2 decade^{-1} or -8.17% decade^{-1} in A2, and -2.67×10^5 km^2 decade^{-1} or -4.78% decade^{-1} in B1. As a result, the average multiyear sea ice areas during 2080–2100 are 0.25×10^7 km^2 in A1B, 0.23×10^7 km^2 in A2, and 0.33×10^7 km^2 in B1, equivalent to reductions of 59.7%, 65.0%, and 45.8%, respectively, relative to the multimodel ensemble means for 1979–99: 0.61×10^7 km^2 in A1B and B1 and 0.67×10^7 km^2 in A2. The multimodel ensemble mean seasonal ice area increases at rates of 1.10×10^5 km^2 decade^{-1} in A1B, 1.99×10^5 km^2 decade^{-1} in A2, and 1.05×10^5 km^2 decade^{-1} in B1, leading to average seasonal ice areas of 0.95×10^7 km^2 in A1B, 1.00×10^7 km^2 in A2, and 0.93×10^7 km^2 in B1 during 2080–2100. The seasonal ice areas are equivalently increased 14.1%, 27.8%, and 11.2%, respectively, relative to the multimodel ensemble means for 1979–99: 0.83×10^7 km^2 in A1B and B1 and 0.78×10^7 km^2 in A2.

Based on a standard statistical analysis of the distributions of computed trends, the 99% confidence intervals are -5.72 to -2.00×10^5 km^2 decade^{-1} in A1B, -7.08 to -2.80×10^5 km^2 decade^{-1} in A2, and -4.20 to -1.14×10^5 km^2 decade^{-1} in B1 for the multiyear ice; and -1.11 to 3.31×10^5 km^2 decade^{-1} in A1B, 0.35 to 3.63×10^5 km^2 decade^{-1} in A2, and -0.67 to 2.77×10^5 km^2 decade^{-1} for the seasonal ice. These intervals show a quantification of uncertainties and give ranges for what the real mean values of multiyear and seasonal ice changes might be. On the other hand, a large subset of the models with almost the same members falls into the 99% confidence intervals for all three SRES scenarios for both the multiyear and seasonal ice, indicating that the models exhibit a great deal of consistency in projecting the multiyear and seasonal ice changes.

Simulations under the SRES scenarios reveal compensation for multiyear sea ice reduction by seasonal sea ice changes, which could lead to significant consequences for the Arctic freshwater budgets and pathways. Altered freshwater exports via Fram Strait and the Canadian Archipelago may have important implications for the Arctic–North Atlantic interactions, as well as for the North Atlantic thermohaline circulation (THC). In particular, the terrestrial and atmospheric hydrological cycles could be enhanced in the global warming scenarios, freshening the Arctic Ocean through increased freshwater input from enhanced river runoff and precipitation (Kattsov et al. 2005, manuscript submitted to *J. Hydrometeor.*). However, salinization resulting from the increased seasonal ice production could complicate the changes in the freshwater budget of the Arctic Ocean.

d. Amplification of the seasonal cycle of sea ice area in the SRES scenarios

We have demonstrated decreases of multiyear sea ice area and increases of seasonal ice area in SRES scenarios, suggesting an enhancement of sea ice loss in melt season and ice growth in freeze-up season. (Note that the changes of sea ice concentration and volume are correlated when the concentration is less than 100%. In sea ice models, when sea ice grows, newly produced sea ice volume is first calculated and then sea ice concentration is generally increased based on the increased sea ice volume and a threshold of thin ice thickness. In this study, we examined large-scale overall sea ice changes. A large area of the Arctic Ocean and the adjacent seas are covered by sea ice with concentration less than 100%, particularly in summer and in the SRES scenarios simulations. So, changes of sea ice area can be a proxy indicator of changes of sea ice growth.) Accordingly, the changes of sea ice cover are seasonally asymmetric. It is therefore interesting to examine the evolution of the sea ice area in all months and associated changes of seasonal cycle in the SRES scenarios. Figure 5 displays the departures of multimodel ensemble mean monthly sea ice areas from corresponding climatological monthly mean values during 1979–99. Substantial decreases occur in all 12 months in the twenty-first century and in all three scenarios. Although the climatological seasonal cycle based on the data from 1979 to 1999 has been removed, obvious seasonal cycles still exist in the sea ice decrease with smaller sea ice reduction in winter than summer. The fluctuations of the departures are readily increased, implying that the embedded seasonal cycle could be amplified.

To make the changes of the seasonal cycle readily apparent, we computed average seasonal cycles of sea ice area based on multimodel ensemble means in consecutive 20-yr windows from 2000 to 2100 in COMMIT and in the three SRES scenarios. Then we subtracted the climatological seasonal cycle computed during the period of 1979–99 from the seasonal cycle in each 20-yr time window in the twenty-first century under different

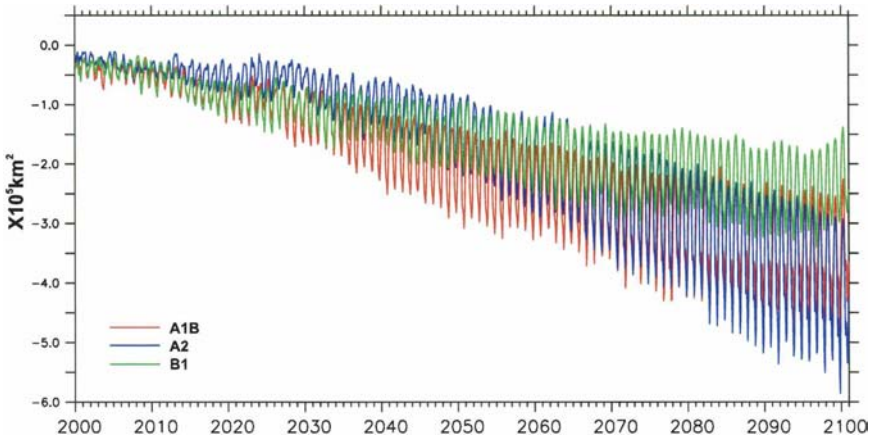

FIG. 5. Projections of multimodel ensemble mean monthly sea ice area anomalies over the Northern Hemisphere from 2000 to 2100, relative to the 1979–99 climatological monthly mean sea ice area. Note that all months' data are included.

scenarios (Fig. 6). Note that the changes for January have been set to zero, so the positive values indicate that a decrease is smaller than in January. The figure clearly illustrates amplitude and phase changes of the seasonal cycle. The COMMIT simulation presents the smallest departures, particularly in winter, relative to the climatology. The relatively small departures of -0.3 to -0.5×10^5 km^2 in summer demonstrate the slightly decreased sea ice areas, coincident with the changes of multimodel ensemble mean annual and multiyear sea ice areas in the same simulations shown in Figs. 3 and 4a. (Recall that several models have projected sea ice area decreases, while other models do not exhibit clear linear trends. The multimodel ensemble mean therefore yields a small decrease of ice area.) The amplitudes of the seasonal cycle in COMMIT vary slightly among

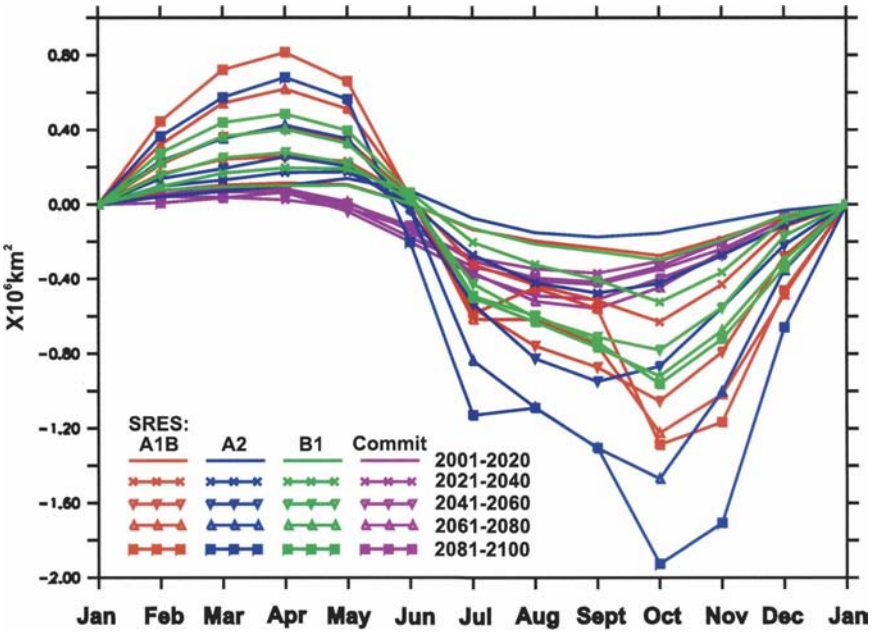

FIG. 6. Departures of averaged sea ice area seasonal cycle from the models' 1979–99 climatology during 20-yr time windows from 2000 to 2100 under the SRES A1B, A2, and B1 and COMMIT scenarios. For convenience in the comparison, the departures in January in all seasonal cycles were adjusted to zero.

the five 20-yr time windows but with no apparent upward or downward trend. This variation appears to result from multidecadal fluctuations.

The seasonal cycles in the SRES A1B, A2, and B1 present very different behaviors from those in the COMMIT simulations (Fig. 6), suggesting significant impacts of the enhanced emissions forcing. The amplitude of the sea ice area seasonal cycle is evidently increased, because the decrease of sea ice area is relatively small in winter and large in summer. The seasonal cycle amplifies with time in each individual SRES scenario; that is, the amplitudes are larger in later time periods than in earlier ones. Comparisons across the SRES scenarios indicate that the seasonal cycle amplifications differ among the SRES scenarios. SRES A1B shows the largest amplifications throughout the year by the middle of the twenty-first century.

In the final 20 yr, the amplitudes (note that it is relative to 0) of the seasonal cycle in SRES A2 increase more rapidly than in B1 in winter, and more rapidly than in A1B in summer. The different seasonal cycle amplification rates may be partially attributable to the nonlinear variations of emissions forcing with time. For example, the CO_2 concentration in A2 is slightly lower than in A1B by the middle of the twenty-first century, while it increases rapidly to a level much higher than in A1B in the second half of the twenty-first century. Additionally, obvious phase changes can be seen in Fig. 6 in the A2 scenario. The curve of sea ice area from June to July shifts to the left in 2080–2100 compared to earlier periods, suggesting an extended melt season.

The absence of a large increase of sea ice area anomalies in August and September in the SRES A1B and A2 during 2061–80 and 2081–2100 is not consistent with the changes of seasonal cycles in these two months during previous time windows, which arises from the constraint of zero ice area. Sea ice areas in a number of models decline dramatically during these two periods or even drop to zero.

4. Summary and discussion

The IPCC has coordinated a comprehensive suite of global climate model simulations using the prescribed emissions forcing observed in the twentieth century (20C3M) and projected for the twenty-first century and beyond (SRES A1B, A2, and B1) for its new assessment report AR4. The three projected emissions forcing scenarios SRES A1B, A2, and B1 that were recommended by the IPCC describe various possibilities for greenhouse gas emissions and provide an unprecedented opportunity for the synthesis of model output in the context of greenhouse forcing. The COMMIT is also a science scenario that assumes that the emissions level will be kept constant throughout the twenty-first century. As a part of international efforts, we focused on an assessment of the global warming impacts on sea ice over the Northern Hemisphere and analyzed all available sea ice concentration data from 15 models in 20C3M, 13 models in SRES A1B and B1, 9 models in SRES A2, and 10 models in COMMIT.

For a credible estimate of sea ice changes, we applied an ensemble mean approach to synthesize modeling results. Ensemble mean for each individual model when ensemble members are available helps to minimize a model's sensitivity to initialization. Use of the multimodel ensemble mean enhances robustness of our estimates of sea ice changes, digging out consistent and common information among various models (note that these models have very diverse treatments in mathematics and physics). Our results demonstrate that the IPCC AR4 models show apparent interannual and decadal variability of sea ice area with various amplitudes. Encouragingly, most of the models' climatological sea ice area, defined in the reference period of 1979–99, is within 20% of the corresponding observational climatology (HadISST1). The climatological seasonal cycle is also simulated well. Moreover, most model simulations show decreasing trends of sea ice area during recent decades, consistent with the observational data. In particular, the multimodel ensemble mean realistically estimates the climatological sea ice area and sea ice area changes during the period of 1979–99, enhancing the credibility of the models' sensitivity to external forcing.

However, large uncertainties still exist in simulating the climate of the twentieth century, particularly in climatological seasonal cycles and long-term changes of simulated sea ice area, as reflected by the large standard deviations in the multimodel ensemble mean. Obvious discrepancies also emerge in a few models. For example, FGOALS-g1.0 greatly overestimates the mean sea ice area, while CNRM-CM3 and CSIRO-Mk3.0 show increasing trends of sea ice areas during 1979–99, opposite to observations and results from most other models. Considering that the FGOALS-g1.0 model is seriously biased in simulating the climate of the twentieth century and does not represent the state of the art, we excluded this model in the analyses of the twenty-first-century sea ice area change projections.

Projections demonstrate an accelerated reduction (relative to 1979–99) in the annual mean sea ice area in the SRES scenarios in the twenty-first century in almost all the IPCC AR4 models. Generally, the largest sea ice area decreases occur in the SRES A1B and A2 and the smallest decreases occur in B1. Changes of sea ice area correspond well to simulated overall surface air tem-

peratures in the various models (CW). A comparison of sea ice area changes between the SRES scenarios and the COMMIT simulations reinforce emissions forcing's impacts. Multimodel ensemble means project the linear decreasing rates of annual mean sea ice areas to be $-3.42\% \pm 1.74\%$ decade^{-1} in A1B, $-3.87\% \pm 1.43\%$ decade^{-1} in A2, and $-2.18\% \pm 1.20\%$ decade^{-1} in B1. This leads to sea ice reductions of 31.09%, 33.39%, and 21.55% under A1B, A2, and B1 scenarios, respectively, relative to those during the period of 1979–99; that is, there are only 0.74×10^7 km^2, 0.73×10^7 km^2, and 0.84×10^7 km^2 of annual mean sea ice area left during the last 20-yr period of the twenty-first century (2080–2100).

The multiyear sea ice area shrinks much more rapidly than the total ice area, and as a consequence the multiyear ice makes the largest contribution to the entire sea ice area loss. In contrast, the seasonal sea ice area generally shows increasing trends. A least squares analysis of the multimodel ensemble means projected changes of $-6.86\% \pm 3.32\%$ decade^{-1}, $-8.17\% \pm 3.44\%$ decade^{-1}, and $-4.78\% \pm 3.05\%$ decade^{-1} for multiyear sea ice area and $1.77\% \pm 2.75\%$ decade^{-1}, $2.87\% \pm 2.21\%$ decade^{-1}, and $1.52\% \pm 2.34\%$ decade^{-1} for seasonal ice area in the A1B, A2, and B1 scenarios, respectively. As a consequence of the opposite-signed changes of multiyear and seasonal sea ice, seasonal cycles of sea ice cover are dramatically amplified and an increased large portion of only seasonally ice-covered Arctic Ocean is expected by the end of the twenty-first century.

The amplification varies among scenarios, with the largest increase of amplitudes in SRES A1B in winter and in SRES A2 in summer. This asymmetry is attributed to the complex interplay between the rate of sea ice retreat and the nonlinearities of emissions forcing changes in the SRES scenarios. The redistribution between multiyear and seasonal ice may have significant implications for energy and freshwater budgets in the Arctic Ocean. In addition, phase changes are also obviously observed in the seasonal cycle of sea ice area in the A2 scenario in the late twenty-first century, indicating an extended melt season.

Large uncertainties still exist in the projected rates of decrease of sea ice area and in the future sea ice cover in the IPCC AR4 models. Based on the multimodel ensemble means, statistical computation produces 99% confidence intervals in various scenarios for the annual mean, multiyear, and seasonal sea ice areas, providing ranges that real mean values of sea ice changes would fall into with 99% confidence. The width of the intervals quantifies uncertainties in estimating sea ice changes. In our analyses, a substantial subset of the participating models falls into the 99% confidence intervals not only within the same SRES scenario but also across scenarios, showing a consistency of these models in projecting sea ice changes and enhancing our confidence in the simulations provided by these models. However, the relatively large width of the confidence intervals we see in this study shows the need for experimental diagnosis of the across-model differences and for further model improvement in order to reduce the uncertainty in the projection.

The attribution of the uncertainties is complex and cannot be rigorously established based on the current available data and information. Nevertheless, we examined the potential impacts of initial sea ice condition on the projection of sea ice changes. The results show a general negative correlation between the annual mean sea ice areas during 1979–99 and the rates of decrease of annual mean sea ice area from 2000 to 2100, suggesting an importance of model simulation for the climate of the twentieth century. However, the simulated feedbacks related to surface albedo, cloud, etc., are possibly quite different depending on the model. These differences could result in varied increases in surface heat budgets and are important for sea ice change projection simulations, which complicate the relationships such as the initial ice area–ice reduction correlation. To detect potential influence of "natural variability" on the projected trends, we checked each ensemble member of the GISS-ER and MRI-CGCM2.3.2 models. Each model's simulated trends were very similar across ensemble members. The across–ensemble member standard deviations are considerable smaller than the across-model values, indicating that the natural variability does not have a major influence on the simulated trends.

This study presents overall sea ice changes over the Northern Hemisphere. Detailed studies of regional sea ice changes for the climate of the twentieth century and projections for global warming scenarios, as well as associated sensitivity studies, will be presented in a follow-up paper.

Acknowledgments. We acknowledge the international modeling groups for providing their data for analysis, the Program for Climate Model Diagnosis and Intercomparison (PCMDI) for collecting and archiving the model data, the JSC/CLIVAR Working Group on Coupled Modelling (WGCM) and their Coupled Model Intercomparison Project (CMIP) and Climate Simulation Panel for organizing the model data analysis activity, and the IPCC WG1 TSU for technical support. The IPCC Data Archive at Lawrence Livermore National Laboratory is supported by the Office of Science, U.S.

Department of Energy. We are grateful to the two anonymous reviewers and editor Andrew Weaver for their constructive comments and suggestions, which improved the presentation and content of this paper. This work was supported by the Japan Agency for Marine-Earth Science and Technology and by the National Science Foundation, Office of Polar Programs, through Grant OPP-0327664. The Arctic Region Supercomputing Center provided part of the computational resources.

REFERENCES

ACIA, 2004: *Arctic Climate Impact Assessment: Scientific Report.* Cambridge University Press, 144 pp.

Bitz, C. M., and W. H. Lipscomb, 1999: An energy-conserving thermodynamic model of sea ice. *J. Geophys. Res.,* **104,** 15 669–15 677.

——, M. M. Holland, A. J. Weaver, and M. Eby, 2001: Simulating the ice-thickness distribution in a coupled climate model. *J. Geophys. Res.,* **106,** 2441–2464.

Cavalieri, D. J., and C. L. Parkinson, 2003: 30-year satellite record reveals contrasting Arctic and Antarctic decadal sea ice variability. *Geophys. Res. Lett.,* **30,** 1970, doi:10.1029/2003GL018031.

Chapman, W. L., and J. E. Walsh, 1993: Recent variations of sea ice and air temperature in high latitudes. *Bull. Amer. Meteor. Soc.,* **74,** 33–47.

Comiso, J., 2002: A rapidly declining perennial ice cover in the Arctic. *Geophys. Res. Lett.,* **29,** 1956, doi:10.1029/2002GL015650.

Hibler, W. D., III, 1979: A dynamic thermodynamic sea ice model. *J. Phys. Oceanogr.,* **9,** 815–846.

Houghton, J. T., Y. Ding, D. J. Griggs, M. Noguer, P. J. van der Linden, X. Dai, K. Maskell, and C. A. Johnson, Eds., 2001: *Climate Change 2001: The Scientific Basis.* Cambridge University Press, 881 pp.

Hunke, E. C., and J. K. Dukowicz, 1997: An elastic–viscous–plastic model for sea ice dynamics. *J. Phys. Oceanogr.,* **27,** 1849–1867.

IPCC, 2001: *Climate Change 2001: Synthesis Report.* Cambridge University Press, 397 pp.

Johannessen, O. M., and Coauthors, 2004: Arctic climate change: Observed and modeled temperature and sea-ice variability. *Tellus,* **56A,** 328–341.

Kwok, R., 2004: Annual cycles of multiyear sea ice coverage of the Arctic Ocean. *J. Geophys. Res.,* **109,** C11004, doi:10.1029/2003JC002238.

Lane, D., 2002: *Hyperstat, 2e.* Atomic Dog Publishing, 236 pp.

Madec, G., and M. Imbard, 1996: A global ocean mesh to overcome the North Pole singularity. *Climate Dyn.,* **12,** 381–388.

Manabe, S., and R. J. Stouffer, 1980: Sensitivity of a global climate model to an increase of CO_2 concentration in the atmosphere. *J. Geophys. Res.,* **85,** 5529–5554.

Murray, R. J., 1996: Explicit generation of orthogonal grids for ocean models. *J. Comput. Phys.,* **126,** 251–273.

Nakicenovic, N., and R. Swart, Eds., 2000: *Special Report on Emissions Scenarios.* Cambridge University Press, 612 pp.

Parkinson, C. L., and D. L. Cavalieri, 2002: A 21-year record of Arctic sea-ice extents and their regional, seasonal and monthly variability and trends. *Ann. Glaciol.,* **34,** 441–446.

——, ——, P. Gloersen, H. J. Zwally, and J. C. Comiso, 1999: Arctic sea ice extents, areas, and trends, 1978–1996. *J. Geophys. Res.,* **104,** 20 837–20 856.

Rayner, N. A., D. E. Parker, E. B. Horton, C. K. Folland, L. V. Alexander, D. P. Rowell, E. C. Kent, and A. Kaplan, 2003: Global analyses of SST, sea ice and night marine air temperature since the late nineteenth century. *J. Geophys. Res.,* **108,** 4407, doi:10.1029/2002JD002670.

Rind, D., R. Healy, C. Parkinson, and D. Martinson, 1995: The role of sea ice in $2\times CO_2$ climate model sensitivity. Part I: The total influence of sea ice thickness and extent. *J. Climate,* **8,** 449–463.

Rothrock, D. A., Y. Yu, and G. A. Maykut, 1999: Thinning of the arctic sea ice cover. *Geophys. Res. Lett.,* **26,** 3469–3472.

Serreze, M. C., and Coauthors, 2003: A record minimum arctic sea ice extent and area in 2002. *Geophys. Res. Lett.,* **30,** 1110, doi:10.1029/2002GL016406.

Stroeve, J. C., M. C. Serreze, F. Fetterer, T. Arbetter, W. Meier, J. Maslanik, and K. Knowles, 2005: Tracking the Arctic's shrinking ice cover: Another extreme September minimum in 2004. *Geophys. Res. Lett.,* **32,** L04501, doi:10.1029/2004GL021810.

Thompson, D. W., and J. M. Wallace, 1998: The Arctic Oscillation signature in the winter time geopotential height and temperature fields. *Geophys. Res. Lett.,* **25,** 1297–1300.

Vinnikov, K. Y., and Coauthors, 1999: Global warming and Northern Hemisphere sea ice extent. *Science,* **286,** 1934–1937.

Wadhams, P., and N. Davis, 2000: Further evidence of the ice thinning in the Arctic Ocean. *Geophys. Res. Lett.,* **27,** 3973–3975.

Zhang, X., M. Ikeda, and J. E. Walsh, 2003: Arctic sea ice and freshwater changes driven by the atmospheric leading mode in a coupled sea ice–ocean model. *J. Climate,* **16,** 2159–2177.